

# An Optomechanical Accelerometer with a High-Finesse Hemispherical Optical Cavity

Yiliang Bao, Felipe Guzmán Cervantes, Arvind Balijepalli, John R. Lawall, Jacob M. Taylor,  
Thomas W. LeBrun, and Jason J. Gorman  
National Institute of Standards and Technology, Gaithersburg, MD, 20899 USA  
Email: gorman@nist.gov, thomas.lebrun@nist.gov

**Abstract**—A new design for an optomechanical accelerometer is presented. The design includes a hemispherical optical cavity that can achieve high finesse and a proof mass that is well-constrained by silicon nitride beams. Based on previous work and analysis, the resolution of the accelerometer will be below 1  $\mu\text{g}/\text{rt-Hz}$ . Novel MEMS fabrication processes have been developed for the accelerometer that provide optimized optical and mechanical elements. The optical cavity in the accelerometer has been characterized and a tunable laser has been locked to the cavity, thereby demonstrating the possibility for closed-loop operation of the accelerometer.

**Keywords**— *accelerometer; MEMS; Fabry-Pérot; optical cavity*

## I. INTRODUCTION

This paper reports on the design, fabrication, and preliminary testing of an optomechanical accelerometer that uses Fabry-Pérot interferometry with a high-finesse optical cavity to transduce acceleration. Accelerometers typically measure the displacement of the proof mass with respect to a local reference using various techniques, including piezoelectric materials, strain gauges, and capacitive sensors. This displacement is then converted to acceleration using information about the sensor's dynamic response, such as the fundamental resonant frequency or the frequency response function. Fabry-Pérot interferometry is a highly sensitive and low uncertainty approach for measuring displacement, making it a compelling candidate for integration in accelerometers. Two mirrors are used to form an optical cavity, one being the proof mass, and a laser is used to measure the relative displacement between the two.

Fabry-Pérot interferometry has been previously demonstrated in a number of MEMS accelerometers. This work can be broken into two groups: fiber-optic cavities [1-5] and vertically oriented cavities [6-8]. The first uses an optical fiber to deliver and collect light while also serving as one mirror of the cavity. Most cavities in this group are plane parallel (i.e., two flat mirrors) although hemispherical cavities (i.e., one concave mirror) are possible [5]. Plane-parallel cavities are only marginally stable meaning that small errors in the perpendicularity of the mirrors allows light to leak from the cavity. This makes it challenging to achieve high-finesse cavities, thereby limiting the sensitivity of the accelerometer. The second group uses two mirrors in a vertical configuration

and are almost always plane-parallel. However, the vertical orientation makes it easier to fabricate high quality optics.

As a result, the goal of the presented work is to develop a vertically oriented optomechanical accelerometer with a hemispherical cavity, which will be more stable than existing plane parallel cavities. This will yield a higher optical finesse and as a result, higher acceleration sensitivity. The design, fabrication, and optical testing of the accelerometer are presented in the following sections.

## II. ACCELEROMETER DESIGN

The design of the optomechanical accelerometer is shown in Fig. 1. Two silicon chips that are fabricated separately are bonded together to make the sensor. The first chip contains a microscale hemispherical mirror that is coated with a high-reflectivity mirror coating on the concave side and an anti-reflective (AR) coating on the flat side. The second chip contains the accelerometer proof mass, which is suspended by silicon nitride beams along the top and bottom edges of the proof mass. The proof mass also has a high-reflectivity mirror coating on the side facing the mirror and an AR coating on the opposite side. There is a recess surrounding the hemispherical mirror, thereby allowing the proof mass to move perpendicular to the surface in both directions. The reflective surfaces on the mirror and proof mass form an optical cavity that can be interrogated with a laser to determine the relative displacement between these two surfaces.

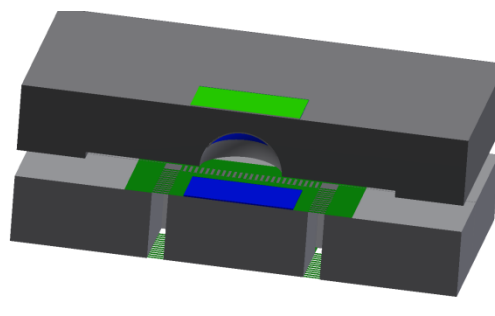


Figure 1: An exploded cross-sectional view of the optomechanical accelerometer showing the hemispherical cavity and suspended proof mass.

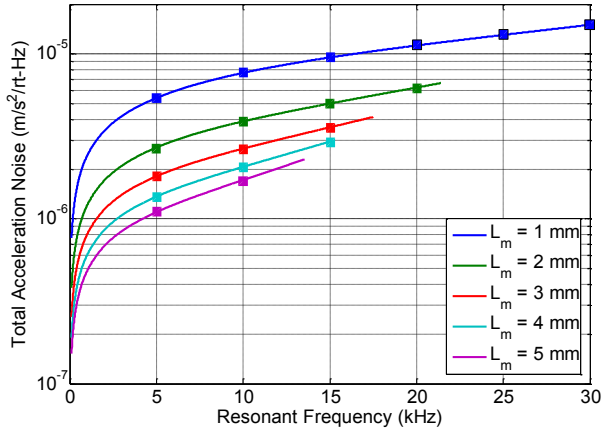


Figure 2: Calculated acceleration noise, including thermal motion and optical detection noise, for varying proof mass size. Squares indicate fabricated accelerometers.

The out-of-plane design was adopted because it allows for the fabrication of a high-quality hemispherical optical cavity that cannot easily be achieved with an in-plane accelerometer. The mechanical beam design, in which the proof mass is suspended on top and bottom, was selected to minimize the influence of rocking modes and to accentuate the piston mode or out-of-plane mode. Finite element analysis has shown that the fundamental mode is the piston mode and the first rocking mode frequencies are at least ten times higher than the fundamental. This frequency separation will result in a sensor with a simple harmonic oscillator response. Finally, with the exception of the silicon nitride beams, mirror coatings, and the AR coatings, the sensor is made of silicon and the bonding of the two chips is between silicon surfaces. As a result, this design should provide excellent thermal stability.

In order to simplify the parameter space, the following values were selected for all designs: beam width,  $w_b = 20 \mu\text{m}$ , beam thickness,  $t_b = 1.5 \mu\text{m}$ , proof mass thickness,  $t_m = 500 \mu\text{m}$ . The stiffness and fundamental resonant frequency are set by selecting the beam length,  $L_b$  ( $40 \mu\text{m}$  to  $110 \mu\text{m}$ ), and the length of the square proof mass,  $L_m$  (1 mm to 5 mm). The noise of the accelerometer will be dominated by the thermal noise (see [9]) and the optical detection noise. In our previous work [5], the displacement detection noise for a microscale optical cavity of similar size with a finesse of  $F = 1600$  was found to be  $2 \times 10^{-16}$  m/rt-Hz. This is converted to acceleration noise by multiplying by the square of the fundamental natural frequency,  $\omega_n^2$ . The thermal noise can be calculated using an equation in [9] and values for the proof mass,  $m$ , the quality factor,  $Q$ , which has been measured to be around 15 in air, and  $\omega_n$ . Taking the root mean square of the two noise sources results in the values shown in Fig. 2 for varying  $L_m$  and  $\omega_n$ . For almost all designs, the noise floor will be below  $1 \mu\text{g}/\text{rt-Hz}$  ( $1 \text{ g} = 9.81 \text{ m/s}^2$ ), demonstrating that the presented optomechanical accelerometer should result in significantly better sensitivity than most other MEMS accelerometers.

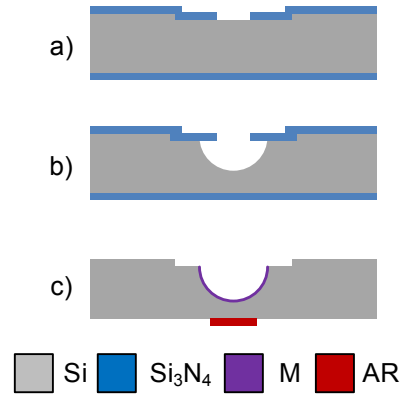


Figure 3: Fabrication process for the hemispherical mirror: a) a recess is etched in Si (DRIE) and is then coated with  $\text{Si}_3\text{N}_4$  (LPCVD), b) aperture is etched in  $\text{Si}_3\text{N}_4$  (RIE) and then Si hemisphere is etched (HNA), c) after removal of  $\text{Si}_3\text{N}_4$ , mirror (M) and antireflection (AR) coatings are deposited using a shadow mask and lift-off process, respectively.

In order to obtain the measurements described in Section IV, free-space optics were used to couple light into the cavity. However, we are now working on a method to assemble the two-chip system into a fiber-optic mount. The same fiber will be used to supply light to the cavity and collect the reflected light. A lens doublet at the end of the fiber will be used to optimize mode matching into the cavity. Cavity coupling will also be optimized by positioning the two-chip system at the location of highest sensitivity relative to the fiber, where it will then be set within the mount using adhesive.

### III. ACCELEROMETER FABRICATION

The fabrication of the two-chip system required the development of unique processes. The hemispherical mirror chip was fabricated using a slow isotropic etch that results in low roughness and high radius of curvature. The process is described in Fig. 3. First, the recess is etched  $10 \mu\text{m}$  deep using deep reactive ion etching (DRIE). The wafer is then coated with LPCVD stoichiometric silicon nitride with a thickness of  $300 \text{ nm}$ , which serves as a mask for the isotropic etch. An aperture is etched through the silicon nitride using reactive ion etching (RIE) for each hemispherical mirror. The wafer is then etched in hydrofluoric, nitric, and acetic acids (HNA) for a predetermined time in order to achieve the desired depth and radius of curvature. This process is based on the one developed by Moktadir et al. [10]. However, much large apertures are used here to achieve fairly long cavity lengths ( $\approx 250 \mu\text{m}$ ) and even larger radii of curvature ( $\approx 350 \mu\text{m}$ ). A highly stable optical cavity is achieved through this ratio of radius of curvature to cavity length. In a final step, the mirror and AR coatings are applied through a shadow mask and lift-off resist, respectively, by an optical coatings vendor.

Fabricated mirrors are shown in Fig. 4. It is clear from the cross-sectional image (Fig. 4b) that the mirror is not a perfect hemisphere, as desired. Optical profilometer measurements were performed on mirrors to determine their surface quality, as shown in Fig. 5. The surface quality is better than  $\lambda/25$  and

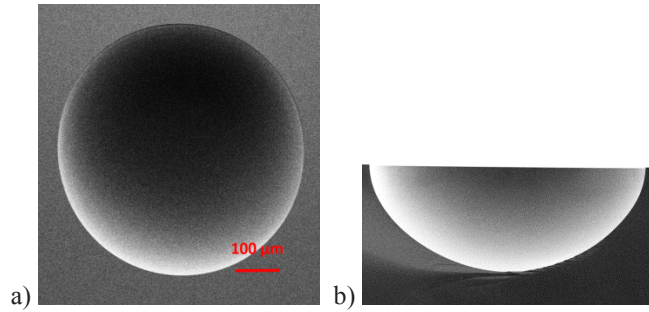


Figure 4: Etched hemispherical mirror: a) top view, b) cross-section.

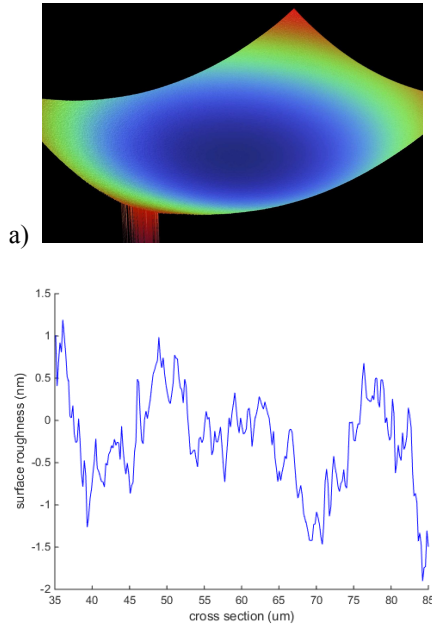


Figure 5: Optical profilometry data for a hemispherical mirror: a) 3D image, b) surface roughness.

the surface roughness is approximately 1 nm RMS, making these exceptional mirrors for interferometry. The roughness can be improved further if necessary through oxidation and etch steps.

The fabrication process for the suspended proof mass is shown in Fig. 6. First LPCVD low stress silicon nitride is deposited on a silicon wafer. The silicon nitride layer is then etched using RIE to leave patches above and below the proof mass location. Mirror and AR coatings are then applied as described above. The beam and proof mass geometry is then etched on both sides until they meet using RIE followed by DRIE. Finally the beams are released by undercutting them using KOH. A released proof mass is shown in Fig. 7.

#### IV. OPTICAL CAVITY MEASUREMENTS

As a step towards fully functional accelerometers, the properties of the microscale optical cavities have been measured. A two-chip system with an unreleased proof mass was used for these measurements. The cavity was interrogated with a tunable diode laser with a nominal wavelength of 1550 nm. The laser was mode matched to the cavity using two

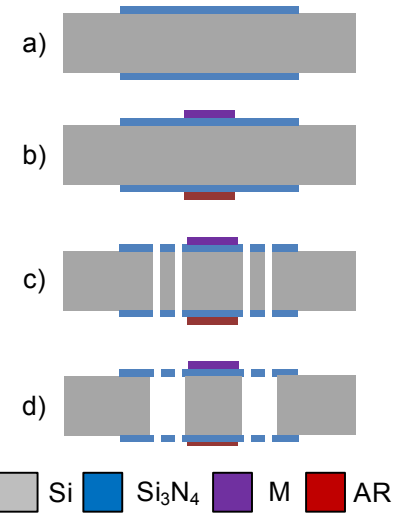


Figure 6: Fabrication process for the suspended proof mass: a)  $\text{Si}_3\text{N}_4$  is deposited on a Si wafer (LPCVD) and patterned, b) mirror (M) and antireflection (AR) coatings are deposited using a lift-off process, c) the proof mass suspension is etched through the  $\text{Si}_3\text{N}_4$  (RIE) and Si wafer (DRIE) on both sides, d) the remaining Si under the  $\text{Si}_3\text{N}_4$  beams is etched (KOH).

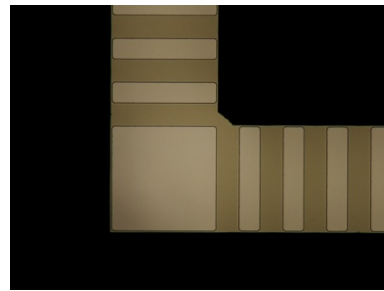


Figure 7: Transmission optical micrograph of the corner of a fabricated suspended proof mass.

lenses and the reflected light was positioned onto a photodetector using a beamsplitter. The accelerometer was positioned relative to the laser using a six-axis motion stage.

After alignment, the wavelength of the laser was scanned using coarse tuning to observe the mode structure of the optical cavity. The fundamental mode is clear and repeats at a fixed interval, as expected (see Fig. 8). This interval is the free spectral range (FSR),  $\text{FSR} = c/2L$ , where  $c$  is the speed of light and  $L$  is the cavity length. The FSR was measured to be 678.12 GHz, indicating a cavity length of 221  $\mu\text{m}$ , which is within the expected range. The finesse of the cavity is estimated to be 2798 based on a slower scan of a resonance (see Fig. 8b).

While there are several ways to measure the relative displacement in the cavity, possibly the most attractive method is to lock a laser to the cavity and then measure the frequency of the laser. The laser frequency changes can then be converted to a displacement. In this work, we have used a dither lock for this purpose. The current supplied to the laser diode was modulated at a single frequency (100 kHz in this

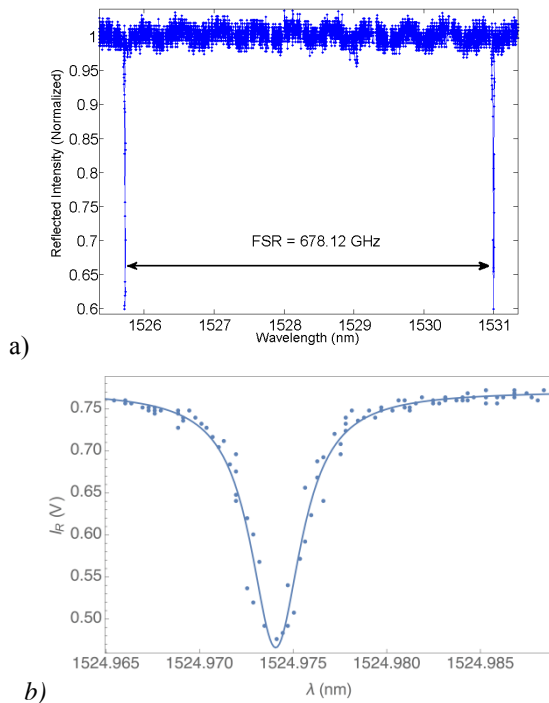


Figure 8: Reflected intensity of the hemispherical optical cavity as a function of wavelength: a) wide wavelength scan showing two adjacent optical modes, b) narrow scan showing a single mode.

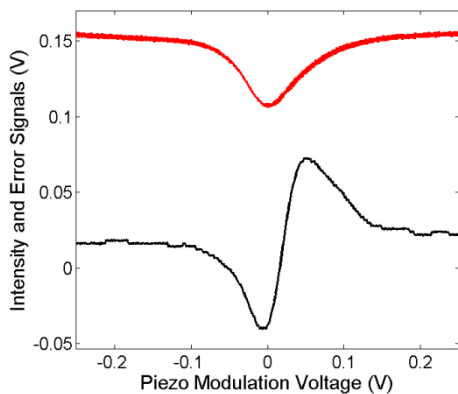


Figure 9: Optical cavity resonance (red) and error signal from lock-in amplifier (black) during a fine wavelength scan. The relationship between piezo voltage and laser frequency is approximately 10 GHz/V.

case) and the signal from the photodetector was processed by a lock-in amplifier. The output of the lock-in amplifier is an error signal that can be used for closed-loop locking of the laser to the cavity. As can be seen in Fig. 9, the error signal is the derivative of the resonance. This data was collected by using the fine wavelength scan (piezo actuator) while providing injection current modulation. The laser was successfully locked to the cavity using this error signal. However, the bandwidth of the laser controller was

insufficient to do an acceleration measurement. We are currently working on an alternative approach for cavity locking that will enable optomechanical sensors with laser frequency readout.

## V. CONCLUSIONS

The design and fabrication of an optomechanical accelerometer with a hemispherical optical cavity has been presented. Based on calculations, the accelerometer is expected to achieve a resolution better than  $1 \mu\text{g}/\text{rt-Hz}$  for a wide range of sensor resonant frequencies, making it highly competitive compared to conventional MEMS accelerometers. The fabricated microscale concave mirrors have been shown to have excellent surface quality (better than  $\lambda/25$ ) and very low surface roughness (1 nm RMS), thereby meeting the requirements for high-finesse optical cavities. An assembled accelerometer was found to have well-defined fundamental modes and an optical finesse around 2800. Using the dither locking technique, we were able to lock a tunable diode laser to the accelerometer.

Two challenges remain before the accelerometer can be used for sensing. The first is stable fiber coupling of the microscale optical cavity. The second is dither locking of the cavity with bandwidth that exceeds that of the fundamental resonant frequency of the accelerometer ( $> 30 \text{ kHz}$ ) while maintaining a large tuning range ( $> \pm 30 \text{ GHz}$ ). These challenges are the focus of our current research.

## ACKNOWLEDGMENT

This research was performed in part in the NIST Center for Nanoscale Science and Technology Nanofab.

## REFERENCES

- [1] G. Schröpfer et al., "Lateral optical accelerometer micromachined in (100) silicon with remote readout based on coherence modulation," *Sens. Actuators, A*, 68, pp. 344-349, 1998.
- [2] M.D. Pocha et al., "Miniature accelerometer and multichannel signal processor for fiberoptic Fabry-Pérot sensing," *IEEE Sens. J.*, 7, pp. 285-292, 2007.
- [3] K. Zandi, J. A. Belanger, and Y.A. Peter, "Design and demonstration of an in-plane silicon-on-insulator optical MEMS Fabry-Pérot-based accelerometer integrated with channel waveguides," *J. Microelectromech. Sys.*, 21, pp. 1464-1470, 2012.
- [4] E. Davies et al., "MEMS Fabry-Pérot optical accelerometer employing mechanical amplification via a V-beam structure," *Sens. Actuators, A*, 215, pp. 22-29, 2014.
- [5] F. Guzmán Cervantes et al., "High sensitivity optomechanical reference accelerometer over 10 kHz," *Appl. Phys. Lett.*, 104, 221111, 2014.
- [6] R.L. Waters and M.E. Aklufi, "Micromachined Fabry-Pérot interferometer for motion detection," *Appl. Phys. Lett.*, 81, pp. 3320-3322, 2002.
- [7] E.J. Eklund and A.M. Shkel, "Factors affecting the performance of micromachined sensors based on Fabry-Pérot interferometry," *J. Micromech. Microeng.*, 15, pp. 1770-1776, 2005.
- [8] M.A. Perez and A. M. Shkel, "Design and demonstration of a bulk micromachined Fabry-Pérot  $\mu\text{g}$ -resolution accelerometer," *IEEE Sens. J.*, 7, pp. 1653-1662, 2007.
- [9] T.B. Gabrielson, "Mechanical-thermal noise in micromachined vibration and acoustic sensors," *IEEE Trans. Electron Devices*, 40, pp. 903-909, 1993.
- [10] Z. Moktadir et al., "Etching techniques for realizing optical micro-cavity atom traps on silicon," *J. Micromech. Microeng.*, 14, pp. S82-S85, 2004.